Electronic Supplementary Material (ESI) for Nanoscale Advances.

Composite Mn-Co electrode materials for supercapacitors: Why the precursor's morphology matters!

Ronan Invernizzi,[a,b] Alexia Lemoine,[c] Lénaïc Madec,[b,c] François Weill,[a,b] Marie-Anne Dourges,[d] Céline Tang, [a,b,e] Domitille Giaume,[b,e] Isabelle Baraille,[b,c] Pierre Louis Taberna,[b,f,g] Delphine Flahaut,[b,c] Jacob Olchowka,*[a,b,f] Liliane Guerlou-Demourgues*[a,b,f]

[a] CNRS, Univ. Bordeaux, Bordeaux INP, ICMCB UMR CNRS #5026, F-33600, Pessac, France.

[b] RS2E, Réseau Français sur le Stockage Electrochimique de l'Energie, FR CNRS #3459, F-80039 Amiens Cedex 1, France.

[d] CNRS/Univ. Pau & Pays Adour / E2S UPPA, Institut des Sciences Analytiques et de Physicochimie pour l'Environnement et les Matériaux − UMR 5254, 64000 Pau, France.

[d] Institut des Sciences Molaires, Univ. Bordeaux, UMR 5255, F-33405 Talence, France

[e] Chimie-ParisTech, PSL Research University, CNRS Institut de Recherche de Chimie-Paris (IRCP), 75005 Paris, France

[f] ALISTORE-ERI European Research Institute, FR CNRS #3104, Amiens, F-80039 Cedex 1, France.

[g] CIRIMAT, Université de Toulouse, CNRS, Université Toulouse 3 – Paul Sabatier, 118 Route de Narbonne, 31062 Toulouse Cedex 9, France

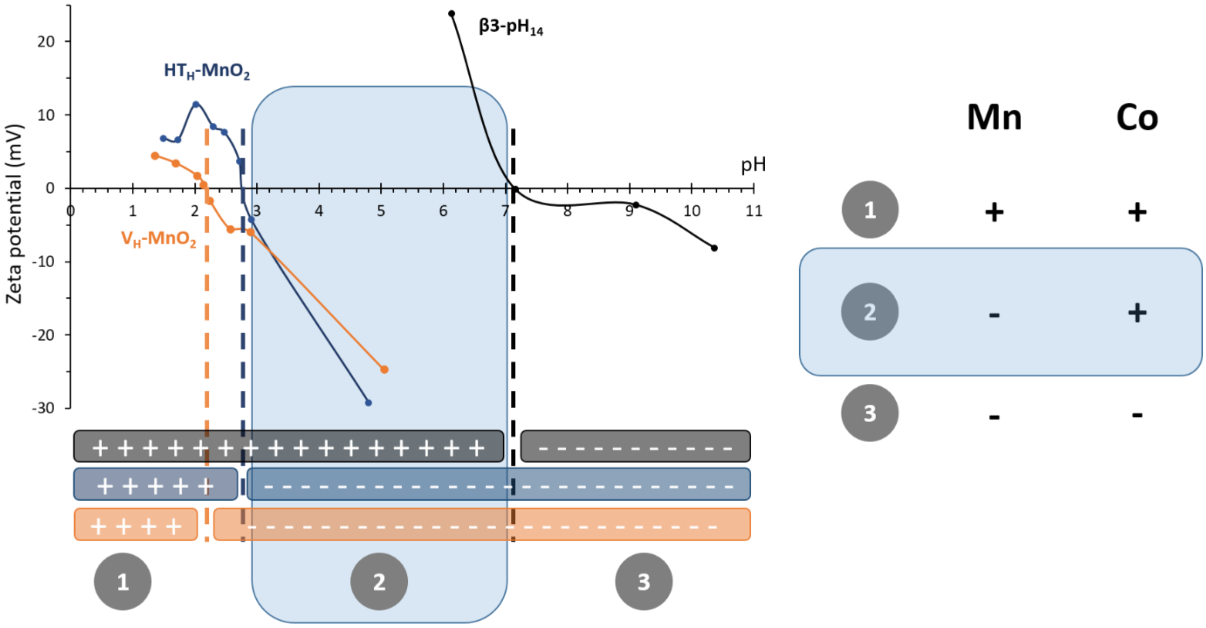

Figure S1. Evolution of Zeta potential of the protonated birnessites and β3-pH$_{14}$.

From these measurements, three domains are defined:

- for pH < 3, the surface of manganese oxides and cobalt oxyhydroxides is positively charged and thus when the particles interact in solution they repeal one each other.

- for 3 < pH < 7, the surface of manganese oxides is negatively charged whereas the surface of cobalt oxyhydroxide is positively charged. In this case, due to their opposite surface charge, the particles are attracted one to each other.

- for pH > 7, the surface of manganese oxides and cobalt oxyhydroxides is negatively charged and thus when the particles interact in solution they repeal one each other.

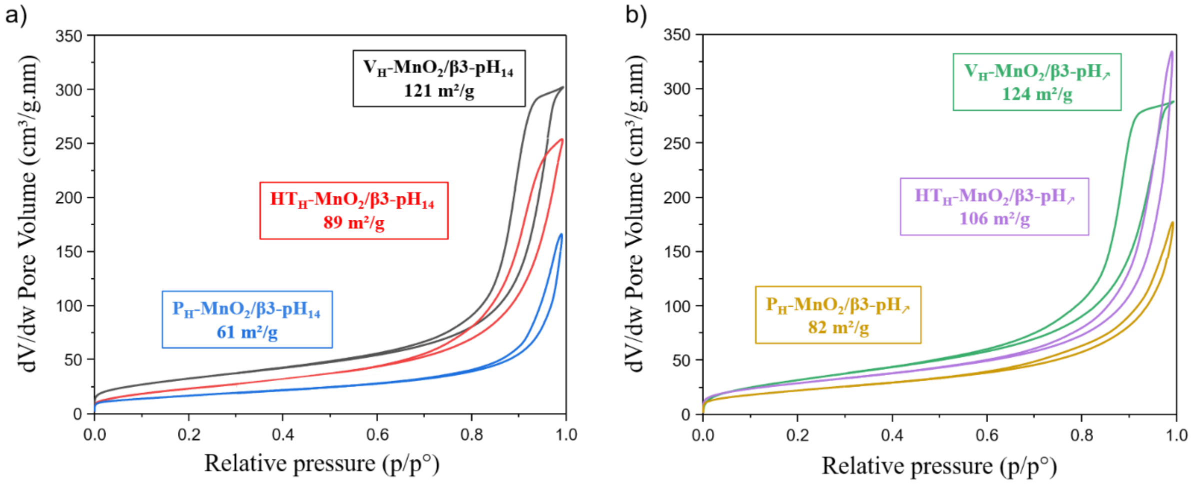

Figure S2 : N_2 adsorption/desorption isotherms at 77 K of a) V_H-MnO_2/β3-pH_{14} (black), HT_H-MnO_2/β3-pH_{14} (red), P_H-MnO_2/β3-pH_{14} (blue) and b) V_H-MnO_2/β3-pH↗ (green), HT_H-MnO_2/β3-pH↗ (purple), P_H-MnO_2/β3-pH↗ (yellow)

By referring to the classification of Sing et al.,[35] the curves obtained on Figure S2 can be classified in two types of isotherms. V_H-MnO_2/β3-pH_{14}, HT_H-MnO_2/β3-pH_{14} and V_H-MnO_2/β3-pH↗ exhibit type IV isotherms, characteristic of mesoporous materials with pore sizes between 2 and 50 nm. The hysteresis loop could be identified as a H3 type, which is very often observed for materials where pores are derived from the aggregation of primary particles with platelet/lamellar morphology,[36] and is consistent with microscopy observations. The application of the BJH model showing the distribution of the pore volume as a function of the pore width confirms the presence of mesoporosity in these 3 composites (Figure S3) with a pore width centered at 17 nm. The other three restacked materials, P_H-MnO_2/β3-pH_{14}, HT_H-MnO_2/β3-pH↗ and $P_H MnO_2$/β3-pH↗, exhibit type II isotherms. They do not show saturation level, and this type of profile corresponds rather to materials with macroporosity and a small mesoporosity probably due to aggregates.

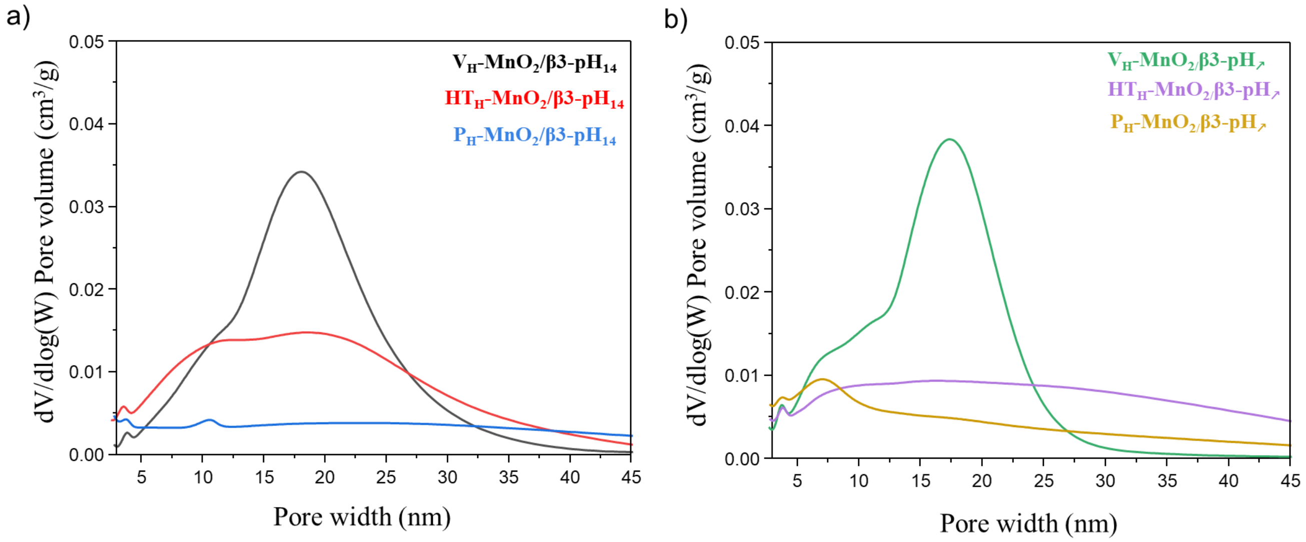

Figure S3 : Comparison of pore size distribution between a) V_H-MnO_2/β3-pH_{14} (black), HT_H-MnO_2/β3-pH_{14} (ref), P_H-MnO_2/β3-pH_{14} (blue) and b) V_H-MnO_2/β3-pH↗ (green), HT_H-MnO_2/β3-pH↗ (purple), P_H-MnO_2/β3-pH↗ (yellow).

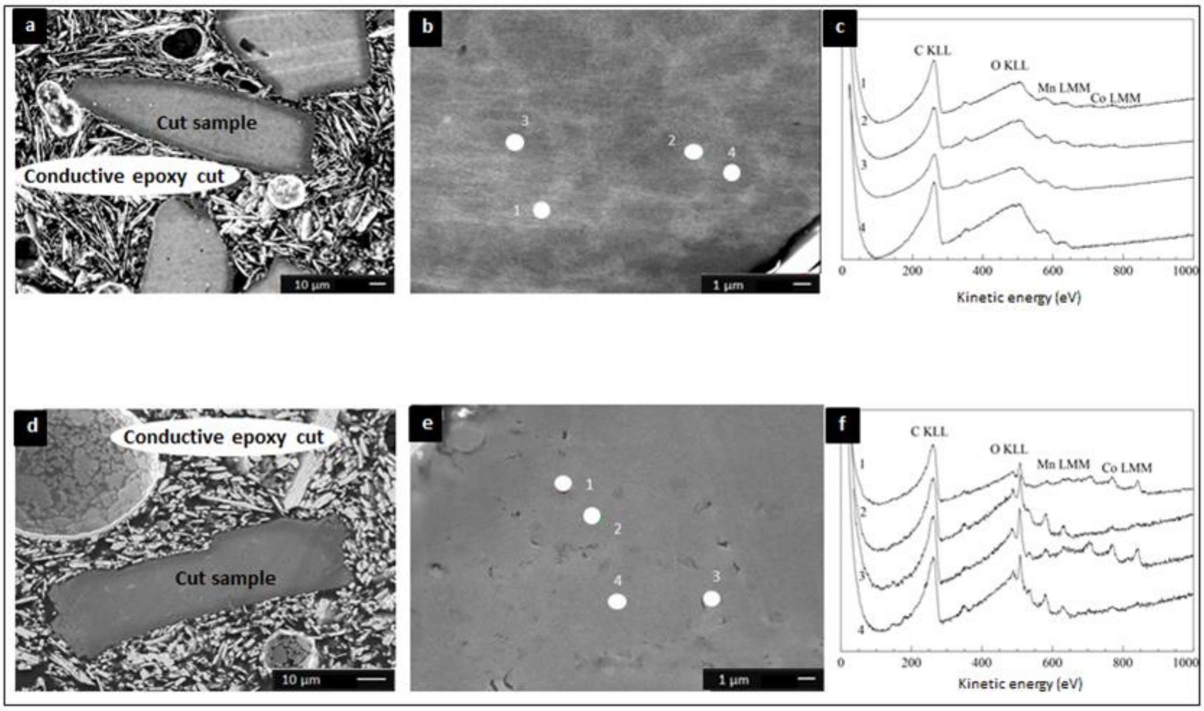

Figure S4: (a,b) SEM images and (c) Auger spectra of restacked material V_H-MnO_2/β3-pH_{14}. (d,e) SEM images and (f) Auger spectra of restacked material V_H-MnO_2/β3-pH↗.

AES spectra (Figure S4c) and S4f) were performed on the different areas marked on SEM images (Figure S4b and S4e) to be representative of the sample. On the Auger spectra, the transitions for O KLL are observed at 500 and 480 eV, for Mn LMM at about 630, 580 and 530 eV and for Co LMM at about 770, 710 and 645 eV.

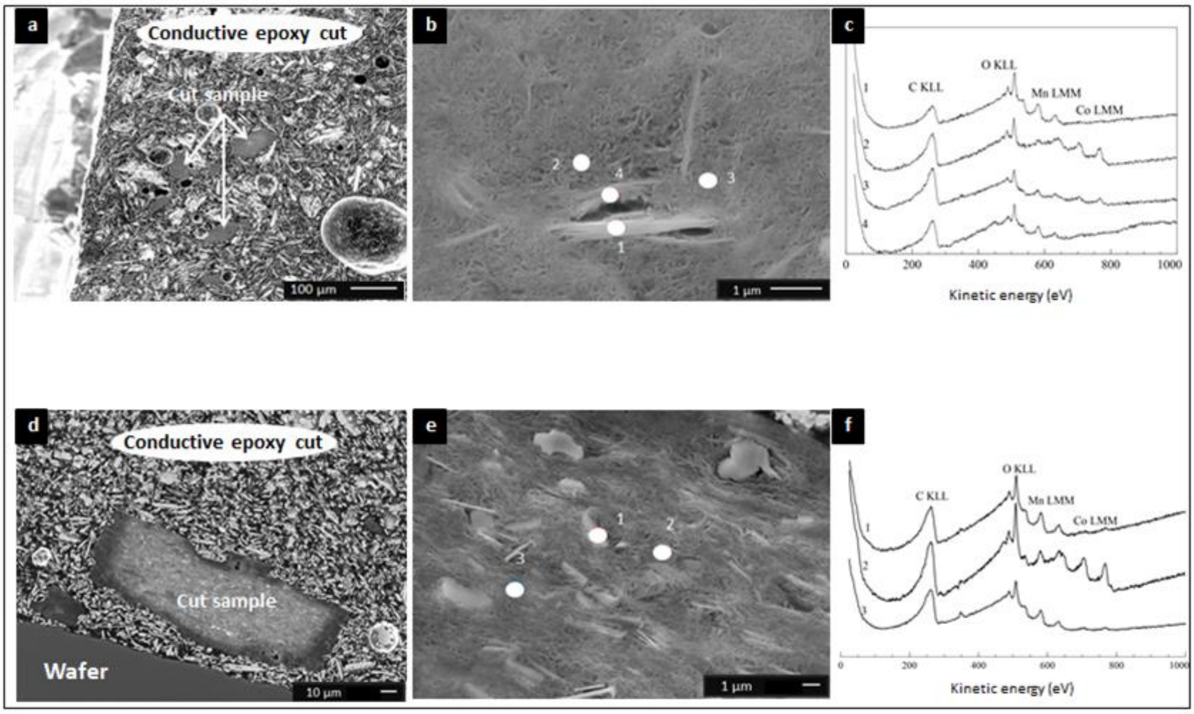

Figure S5: (a,b) SEM images and (c) Auger spectra of restacked material HT_H*-*MnO_2*/β3-*pH_{14}*. (d,e) SEM images and (f) Auger spectra of restacked material* HT_H*-*MnO_2*/β3-*$pH_{\nearrow}$*.*

AES spectra (Figure S5c) and S5f) were performed on the different areas marked on SEM images (Figure S5b and S5e) to be representative of the sample. On the Auger spectra, the transitions for O KLL are observed at 500 and 480 eV, for Mn LMM at about 630, 580 and 530 eV and for Co LMM at about 770, 710 and 645 eV.

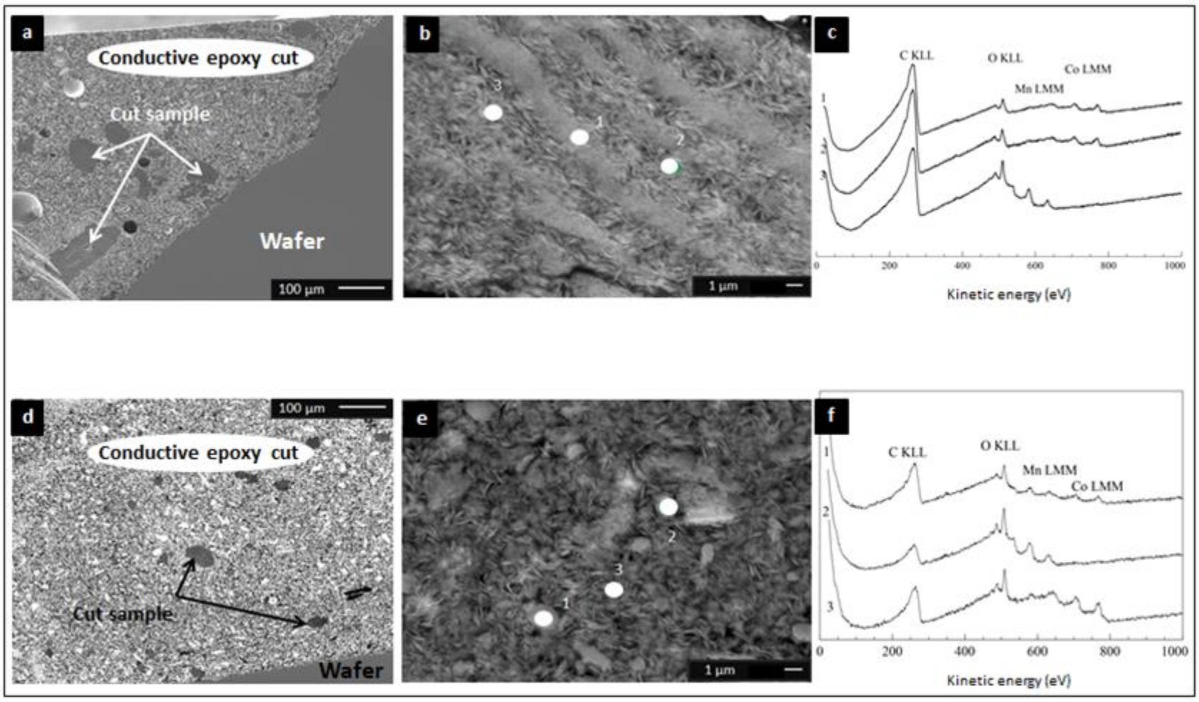

Figure S6: (a,b) SEM images and (c) Auger spectra of restacked material P_H-MnO_2/β3-pH_{14}. *(d,e) SEM images and (f) Auger spectra of restacked material* P_H-MnO_2/β3-$pH_{\nearrow}$.

AES spectra (Figure S6c) and S6f) were performed on the different areas marked on SEM images (Figure S6b and S6e) to be representative of the sample. On the Auger spectra, the transitions for O KLL are observed at 500 and 480 eV, for Mn LMM at about 630, 580 and 530 eV and for Co LMM at about 770, 710 and 645 eV.

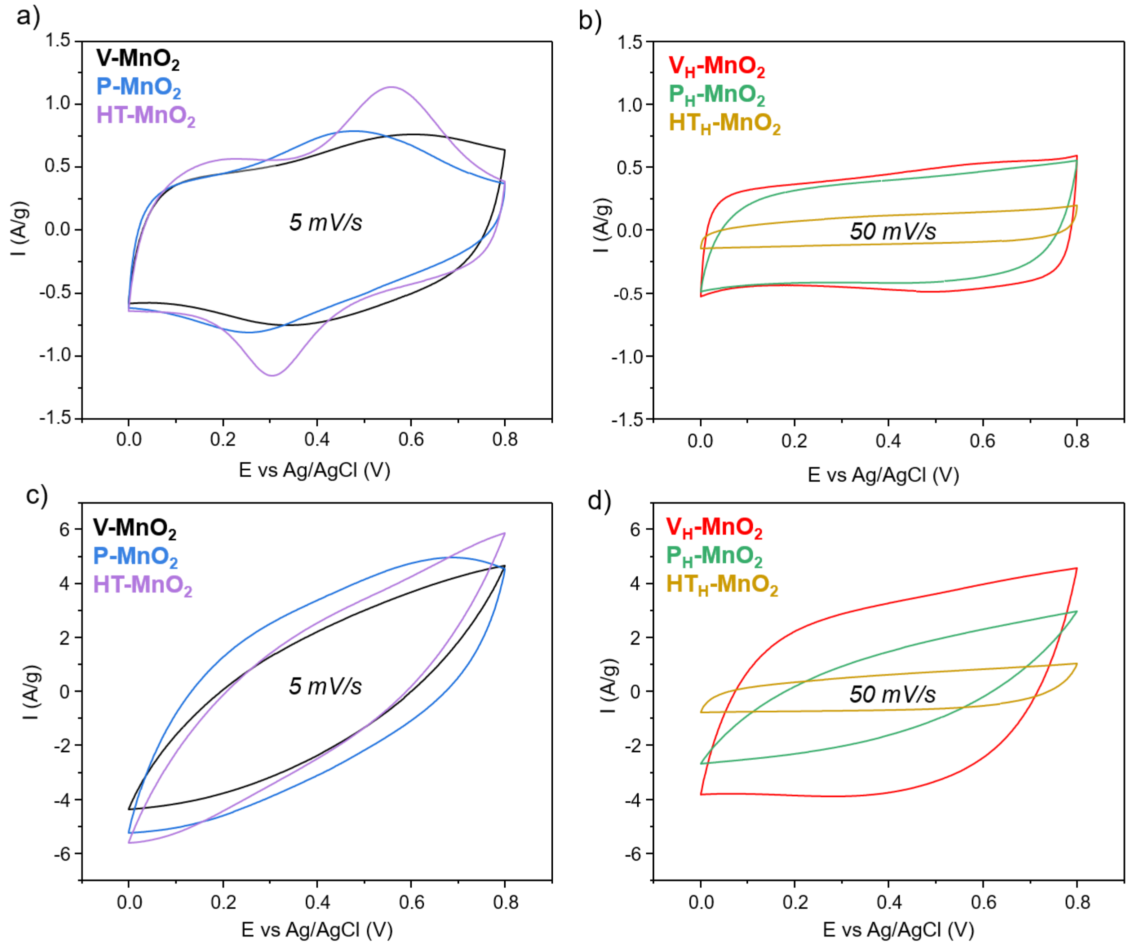

Figure S7. Cyclic voltammetry of initial and protonated birnessites at different scan rates on the potential window 0-0.8 V vs Ag/AgCl in 0.5 M K_2SO_4.

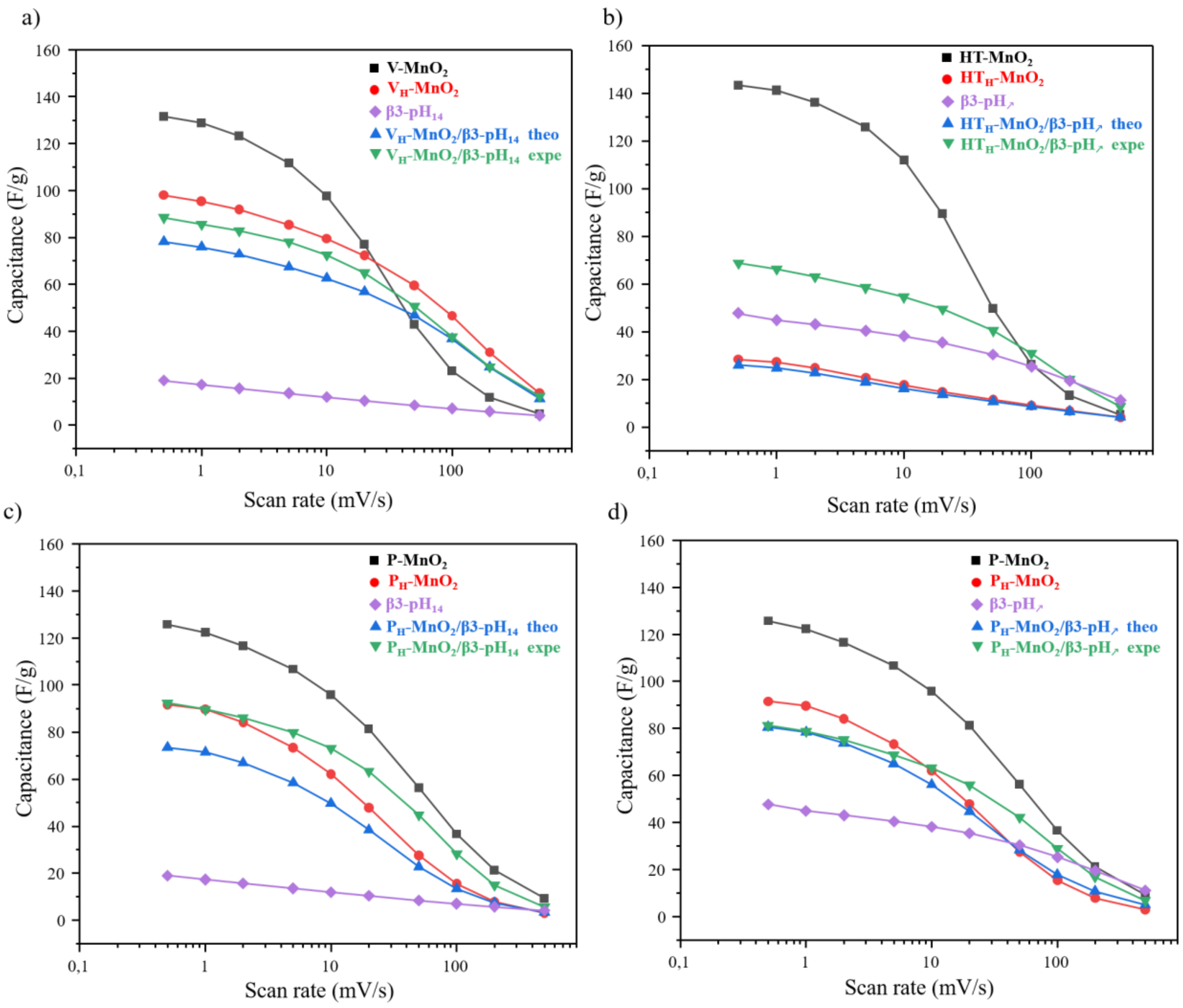

Figure S8. Comparison of the capacitance at different scan rates for the precursors constituting the restacked material with the theoretical and experimental capacitance of the restacked composites a) V_H-MnO_2/β3-pH_{14}, b) HT_H-MnO_2/β3-pH↗, c) P_H-MnO_2/β3-pH_{14}, and d) P_H-MnO_2/β3-pH↗.

The "theoretical" capacity is the weighted average capacity of Co and Mn precursors composing the restacked material and can be written as [3*(capacitance of protonated MnO_2) + 1*(capacitance of cobalt oxyhydroxide)]/4 as each composite possesses a molar ratio Mn:Co of 3:1.

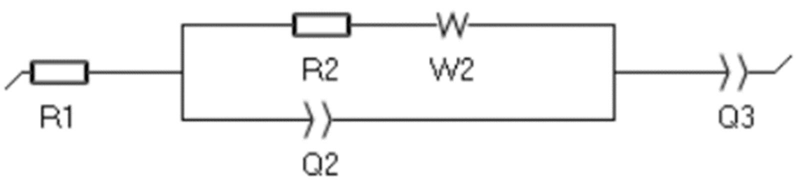

Figure S9. Equivalent circuit used to fit the impedance spectra.

R1 represents electrolyte resistance, R2 the resistance charge transfer, W2 the Warburg element, Q2 and Q3 are constant phase elements. Active material percolation is characterized by R2, W2 and Q2 whereas Q3 represents active material capacitance.

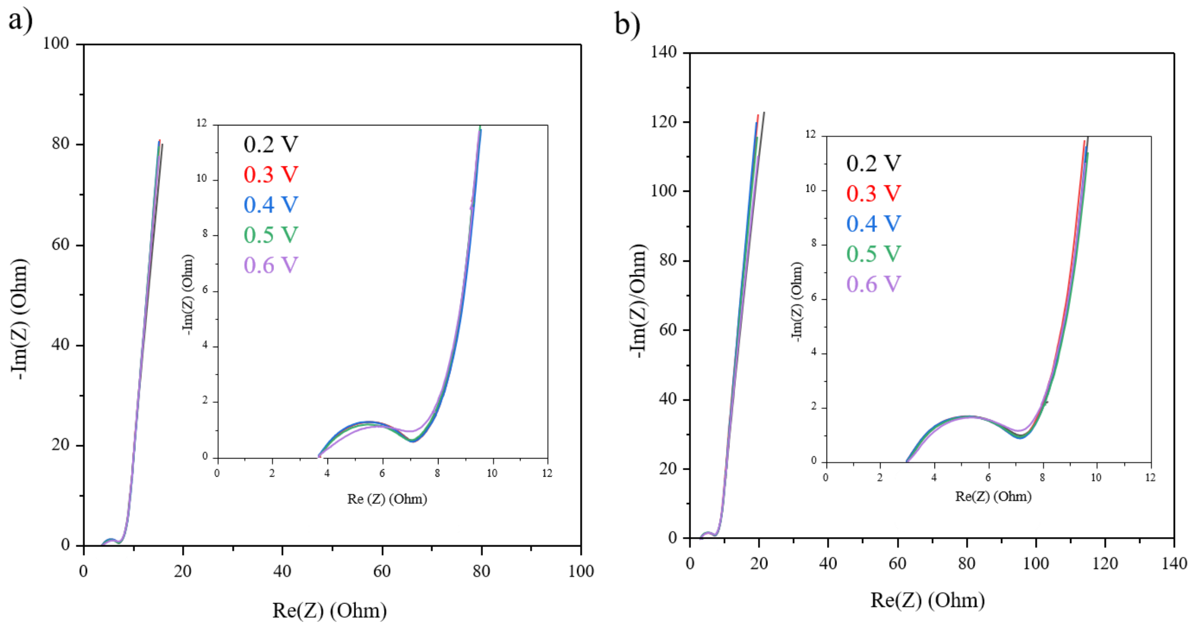

Figure S10. EIS data Nyquist plots of the restacked materials a) V_H-MnO_2/β3-pH↗, b) HT_H-MnO_2/β3-pH_{14} from 0.2 to 0.6 V.

The V_H-MnO_2/β3-pH↗ and HT_H-MnO_2/β3-pH_{14} composites have been tested at potentials 0.2-0.3-0.4-0.5 and 0.6 V, vs Ag/AgCl, on stainless steel collectors recovered by a thin gold film, on a frequency range of 10 kHz to 10 mHz in 0.5 M K_2SO_4.

Table S1. Composition of initial and protonated precursors

Sample	Chemical composition (wt %)			Molar ratios		Mean oxidation state of transition metal oxide	Chemical formula
	H	**Na/K**	**Mn/Co**	$\frac{H}{Mn/Co}$	$\frac{Na/K}{Mn/Co}$		
V-MnO_2	0.9	8.1	47.2	0.89	0.25	3.52	$H_{0.23}^{+}K_{0.25}^{+}(H_2O)_{0.33}Mn^{3.52+}O_2$
V_H-MnO_2	1.1	0.9	51.3	1.05	0.02	3.63	$H_{0.35}^{+}K_{0.02}^{+}(H_2O)_{0.35}Mn^{3.63+}O_2$
P-MnO_2	1.0	6.6	48.7	1.04	0.32	3.54	$H_{0.14}^{+}Na_{0.32}^{+}(H_2O)_{0.45}Mn^{3.54+}O_2$
P_H-MnO_2	1.1	0.2	56.4	1.12	0.01	3.65	$H_{0.34}^{+}Na_{0.01}^{+}(H_2O)_{0.39}Mn^{3.65+}O_2$
HT-MnO_2	0.6	10.2	45.1	0.64	0.30	3.70	$K_{0.30}^{+}(H_2O)_{0.32}Mn^{3.70+}O_2$
HT_H-MnO_2	1.0	2.7	47.9	1.04	0.08	3.72	$H_{0.20}^{+}K_{0.08}^{+}(H_2O)_{0.42}Mn^{3.72+}O_2$
β3-pH_{14}	1.1	1.7	56	1.09	0.06	3.15	$H_{0.79}^{+}Na_{0.06}^{+}(H_2O)_{0.15}Co^{3.15+}O_2$
β3-pH↗	1.9	3.2	54	1.65	0.15	3.20	$H_{0.65}^{+}Na_{0.15}^{+}\ (H_2O)_{0.50}Co^{3.20+}O_2$

The accurate compositions of all alkaline and protonated birnessite and cobalt oxyhydroxides have been determined by combining ICP-OES, iodometric titrations and CHNS analyses which allow to determine respectively the cationic content (Na, K, Mn), the manganese/cobalt mean oxidation state and the hydrogen content (proton + water).[1]

Table S2. Mn/Co molar ratio determined by ICP-OES for the restacked materials.

Sample	Molar ratio Mn :Co
V$_H$-MnO$_2$/β3-pH$_{14}$	3:1
HT$_H$-MnO$_2$/β3-pH$_{14}$	3:1
P$_H$-MnO$_2$/β3-pH$_{14}$	3:1
V$_H$-MnO$_2$ β3-pH$_{↗}$	3:1
HT$_H$-MnO$_2$/β3-pH$_{↗}$	3:1
P$_H$-MnO$_2$/β3-pH$_{↗}$	2.9:1

Table S3. Summary of values obtained after fitting for V$_H$-MnO$_2$/β3-pH$_{↗}$ and HT$_H$-MnO$_2$/β3-pH$_{14}$ at 0.3 V.

	V$_H$-MnO$_2$/β3-pH$_{↗}$	HT$_H$-MnO$_2$/β3-pH$_{14}$
R1	3.735 Ohm	3.016 Ohm
R2	3.435 Ohm	4.224 Ohm
s2	1.724 Ohm.s$^{-1/2}$	2,065 Ohm.s$^{-1/2}$
Q2	0.998 7e-3 F.s $^{a-1}$	1.195e-3 F.s $^{a-1}$
a2	0,777	0,8171
Q3	0.219 1 F.s $^{a-1}$	0.140 1 F.s $^{a-1}$
a3	1	1

(1) Invernizzi, R.; Guerlou-Demourgues, L.; Weill, F.; Lemoine, A.; Dourges, M.-A.; Baraille, I.; Flahaut, D.; Olchowka, J. Controlled Nanostructuration of Cobalt Oxyhydroxide Electrode Material for Hybrid Supercapacitors. Materials 2021, 14 (9), 2325.